Pol. J. Environ. Stud. Vol. XX, No. X (XXXX), 1-9
DOI: *10.15244/pjoes/214087* ONLINE PUBLICATION DATE: 2026-05-22

Original Research

Phosphorus Removal by Concrete-Based Layered Double Hydroxides: Efficiency and Mechanism

Tingjuan Feng, Xiao Liu*, Yang Li, Yaze Zhi, Yong Yang, Lin Liu, Mei Yang

Center for Water Quality and Ecology, College of Civil and Architectural Engineering, North China University of Science and Technology, Tangshan, 063000, China

Received: 28 August 2025
Accepted: 08 November 2025

Abstract

Phosphorus is a crucial contaminant in controlling water eutrophication. In this study, concrete-based layered double hydroxides (C-LDH/C-LDO) were synthesized to remove phosphorus from water. The main factors influencing phosphorus removal – such as initial pH, contact time, and coexisting anions – were examined, and the removal mechanism was analyzed. Results indicated that C-LDH and C-LDO performed better in acidic conditions, with C-LDO showing superior phosphorus uptake, achieving a maximum adsorption of 164.01 mg/g at 20°C. CO_3^{2-} competitively inhibited phosphorus removal by C-LDH and C-LDO, while NO_3^-, Cl^-, and SO_4^{2-} had less impact. The phosphorus removal mechanisms of C-LDH and C-LDO include electrostatic attraction, interlayer anion exchange, complexation, and chemical precipitation. Overall, C-LDH and C-LDO offer inexpensive and sustainable options for phosphorus removal.

Keywords: waste concrete, layered double hydroxides, phosphorus removal, adsorption isotherm, mechanism

Introduction

As a limiting nutrient for water eutrophication, a phosphorus concentration of 0.2 mg/L [1] can induce water eutrophication [2]. Since the discharge of phosphorus-containing sewage is a major source of phosphorus pollution in the water environment [3], the requirements for phosphorus removal from wastewater are becoming increasingly stringent worldwide.

The general methods for phosphorus removal from wastewater include chemical precipitation [4], biological absorption [5], and medium adsorption, among which medium adsorption proves to be efficient, easy to operate, and cost-effective. Medium adsorption is particularly suitable for high-phosphorus wastewater, which often comes from industries related to phosphate rock, phosphate chemicals, and phosphogypsum, and is usually acidic.

Recently, the efficient adsorption of phosphorus by layered double hydroxides (LDHs) has garnered considerable attention [6, 7]. LDHs have a layered structure similar to brucite, consisting of positively charged lamellae and interlayer anions. The chemical formula is $M_{1-x}^{2+} M_x^{3+}(OH)_2 \left(A^{n-}\right)_{x/n} \cdot mH_2O$. Where M^{2+} is a divalent cation, M^{3+} is a trivalent cation; A^{n-}

*e-mail: hblg0822@163.com

is an intercalated anion between laminates; the range of x is usually between 0.2 and 0.33. The laminates of LDHs are positively charged, which attract interlayer A^{n-} through electrostatic attraction. In addition, the laminates can also bind with interlayer OH^- and H_2O molecules through hydrogen bonding, thereby maintaining the LDHs' electrical neutrality [8, 9]. LDHs have a large specific surface area and strong anion exchange performance, making them promising adsorbents for phosphorus removal [10, 11]. However, most studies used chemical reagents to synthesize LDHs, and the synthesis conditions are relatively strict, which limits the application of LDHs. Therefore, lower material costs and simple synthesis methods are significant.

The hardened concrete's chemical composition includes essential elements like Ca and Al, vital for LDHs synthesis. It is an ideal, low-cost material for LDHs preparation. However, there is no reported research, either domestically or internationally, on this topic. Hence, in this study, C-LDH was synthesized from waste concrete for phosphorus removal to decrease phosphorus removal costs. The study investigated phosphorus removal characteristics, primary influencing factors, and the phosphorus removal mechanism of C-LDH.

Materials and Methods

Materials

Waste concrete is collected from the local civil engineering laboratories after years of crushing and stockpiling. The solution was prepared with ultrapure water to avoid contamination, and the chemicals used were analytically pure.

Synthesis of C-LDHs

The waste concrete underwent a process where it was crushed, and the primary components, such as O, Ca, Si, Mg, Al, and Fe, comprised 36.8%, 28.2%, 11.6%, 5.2%, 4.8%, and 3.4% respectively. The waste was sieved through a 200-mesh sieve, mixed with 1 M hydrochloric acid at a solid-liquid ratio of 1:20, and combined with 1/6 of the concrete mass in $AlCl_3 \cdot 6H_2O$. The mixture was stirred at 40ºC and 180 r/min for 8 hours. Subsequently, the mixture was filtered using a 0.22 μm filter membrane to separate the slag from the filtrate. The filtrate was then transferred to a three-necked bottle containing distilled water, where the pH was maintained at 12 by adding the filtrate and 2 M NaOH solution drop by drop simultaneously. After titration, stirring was continued for 1 hour. The precipitate was washed, filtered, dried, and milled at 65ºC to obtain C-LDH. Finally, the C-LDH was baked at 450ºC to yield the C-LDO product.

Phosphorus Removal

Adjust the raw water series containing 250 mg/L using either 0.1 M HCl or 0.1 M NaOH solution to achieve varying pH levels. Introduce C-LDH to the raw water at different initial pH levels based on a solid-liquid ratio of 1:1000. Allow adsorption to occur at 293 K and 200 r/min for 24 hours to assess residual phosphorus concentration and determine the optimal pH. Explore the coexistence of ions, adsorption kinetics, and adsorption isotherms at the identified optimum pH for further analysis. Phosphorus adsorption is calculated as follows:

$$Q_e = \frac{V(C_0 - C_e)}{M} \tag{1}$$

where V is the volume of the water sample (L), C_0 and C_e are the raw water phosphorus concentration and residual phosphorus concentration (mg/L), respectively, and M is the sample mass (g).

Consequential Extraction of Phosphorus

When comparing Williams [11] and Sommers [12] in a bypass extraction method, the phosphorus removal products of C-LDH and C-LDO were sequentially extracted. Initially, exactly 0.8 g of phosphorus hydrotalcite sample was taken and combined with 100 mL of 0.5 M $NaHCO_3$ solution. The extraction was done by shaking at 20ºC and 150 r/min for 16 hours. The filtrate was filtered, and the residue was washed with KCL solution and distilled water, respectively. The filtrate was then combined with the washing solution to determine the phosphorus concentration. This total extracted phosphorus was noted as loosely bound phosphorus (W-P). The residue from the previous centrifugation step was added to the NaOH solution and further extracted by shaking. The same extraction method was repeated to obtain iron/aluminum-bound phosphorus (Fe/Al-P). The hydrochloric acid solution was then added to the residue from the previous centrifugation step, and the extraction was repeated to obtain calcium/magnesium-bound phosphorus (Ca/Mg-P). Finally, the residue was dried, moved to a beaker containing concentrated hydrochloric acid, and extracted by shaking at 80ºC and 150 r/min for 20 minutes. The extraction was continued at room temperature for 1 hour to obtain strongly bound phosphorus/stabilized phosphorus (S-P).

Analytical Method

P concentration was determined by molybdenum antimony resistance spectrophotometry [13]. The morphology of C-LDH/C-LDO was observed by scanning electron microscopy (SEM, Zeiss Supra55(VP), Germany), and X-ray diffraction (XRD) spectra were

obtained by D/MaX2500PC X-ray diffractometer under 40 kV,100 mA, Cu/kα radiation. Fourier transform infrared (FTIR) spectra of the samples were recorded by the KBr method (IRaffini-1S, Japan).

Results and Discussion

Adsorption Properties

Influence Factors

pH conditions and coexisting anions are the major factors affecting phosphate removal [14]. The rises or declines in pH value cause deprotonation or protonation, which results in the increased repulsion or attraction between the LDHs and phosphate anions, thereby affecting the adsorption of phosphate [15-18]. In addition, a strongly acidic environment will partially dissolve LDHs [19], as shown in reaction (2), resulting in decreased phosphorus removal. Phosphate anions often coexist with other inorganic anions such as NO^{3-}, Cl^-, SO_4^{2-}, and CO_3^{2-}, which often participate in the interlayer adsorption of LDHs. The selectivity of LDHs for anions is related to the ratio of charge to radius: anions with higher valence and smaller radius are more competitive [20]. CO_3^{2-} and SO_4^{2-} were considered to have higher selectivity to LDHs due to their smaller radius and higher charge density [21].

Fig. 1a) demonstrates that C-LDH exhibits a maximum phosphate adsorption capacity at pH 4, achieving a phosphate removal efficiency of 33%. As the initial pH increased, the phosphorus removal efficiency declined sharply and subsequently stabilized. C-LDO displayed comparable trends in phosphorus removal efficiency across varying pH conditions. The experimental results collectively indicate that C-LDH/C-LDO systems exhibit broad pH adaptability, with superior phosphorus removal performance under acidic conditions compared to alkaline environments. This enhanced efficiency under acidic conditions is attributed to two synergistic mechanisms: Firstly, surface protonation under acidic conditions intensifies electrostatic attraction between the material surface and PO_4^{3-}. Secondly, increased solubility at lower pH promotes the dissolution of multivalent cations, which subsequently enhances phosphate precipitation through chemical interactions (as described in reaction (2)).

$$\left[M^{II}_{a(1-x)}M^{III}_{bx}(OH)_2\right]^{x+}\left[A^{n-}_{\frac{x}{n}}\cdot yH_2O\right]^{x-}(s) \rightleftharpoons (1\text{-}x)M^{2+}_a(aq) + xM^{3+}_b(aq) + \frac{x}{n}A^{n-} + 2OH^- + yH_2O \quad (2)$$

Fig. 1b) shows that when the raw water phosphorus concentration is 250 mg/L, the phosphorus removal effects of C-LDH and C-LDO are less affected by NO^{3-}, Cl^-, and SO_4^{2-}, but are affected by CO_3^{2-}. It is obvious that a high concentration of CO_3^{2-} will significantly weaken the phosphorus removal effect.

It can be seen from formula (3) that a large amount of CO_3^{2-} in the solution system will shift the ionization equilibrium to the right, thereby reducing the overall positive charge and weakening electrostatic adsorption, which is not conducive to phosphorus removal.

$$CO_3^{2-} + H_2O \rightleftharpoons HCO_3^- + OH^- \quad (3)$$

Significantly, even if 200 mg/L CO_3^{2-} coexists, the phosphorus removal rate of C-LDH/C-LDO only decreases by about 10%, and the phosphorus removal effect is still significant.

Adsorption Kinetics

In kinetic studies, the adsorption capacity of the adsorbent was investigated as a function of time. The experimental data were fitted using the pseudo-first-order kinetic Equation (4) and the pseudo-second-order kinetic Equation (5), and the corresponding expression is:

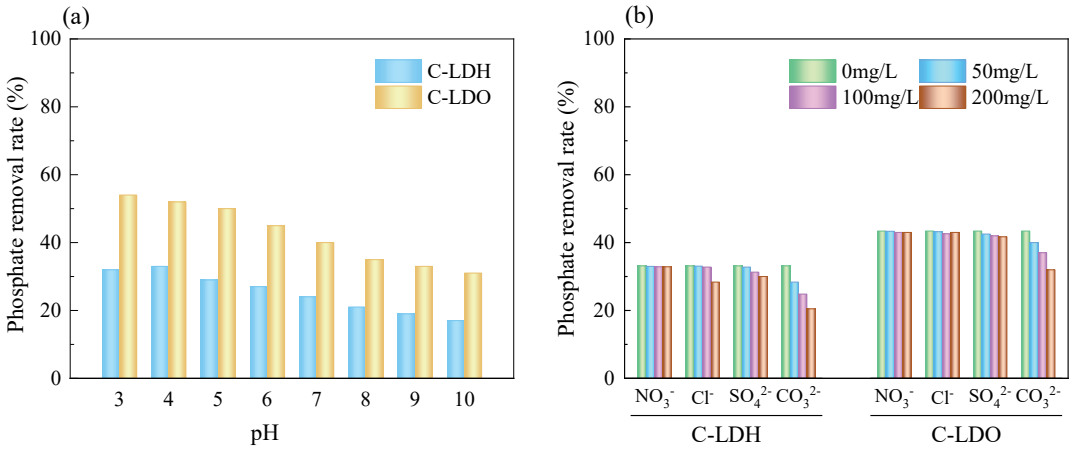

Fig. 1. Influences of pH and coexisting ions on phosphorus removal. a) C-LDH and b) C-LDO.

$$\ln(Q_e - Q_t) = \ln Q_e - k_1 t \quad (4)$$

$$\frac{t}{Q_t} = \frac{1}{Q_e^2 k_2} + \frac{t}{Q_e} \quad (5)$$

where Q_t is the adsorbed amount at time t (mg/g), Q_e is the adsorbed amount at reaction equilibrium (mg/g), K_1, K_2 are the rate constants (min^{-1}), and t is the adsorption time (h).

The pseudo-first-order and pseudo-second-order kinetic models were applied to fit the adsorption processes of C-LDH and C-LDO (Fig. 2). The kinetic parameters derived from the applied kinetic models are summarized in Table 1.

Fig. 2 and Table 1 show that the experimental data better match pseudo-second-order kinetics (R^2>0.98), indicating that the phosphorus adsorption by C-LDH/C-LDO was controlled by both physical adsorption and chemical adsorption [22]. It can be observed from Fig. 2 that the phosphate adsorption by C-LDH/C-LDO occurs in two distinct stages. In the initial stage, the adsorption proceeds rapidly, while the rate decreases significantly in the subsequent stage. During the early phase of adsorption, phosphate ions are primarily adsorbed onto the surface of the concrete-based hydrotalcite materials. As the process continues, the ions diffuse into the pore structure, adsorb onto the internal pore walls, and gradually fill the pore channels. With progressive saturation of the available adsorption sites, the concentration gradient diminishes, leading to a reduced adsorption rate [23]. The phosphorus adsorption behavior of C-LDH/C-LDO aligns more closely with pseudo-second-order kinetic models. This suggests that surface adsorption governed by chemical interactions may represent the primary rate-limiting mechanism influencing the overall adsorption process [24].

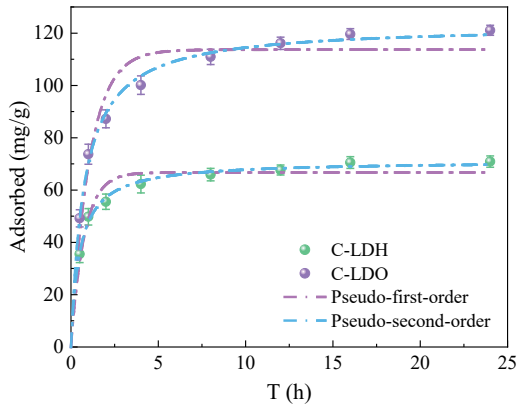

Fig. 2. Kinetic fitting of phosphorus removal by CLDH and CLDO adsorption.

Adsorption Isotherms

The Langmuir model and the Freundlich model are classic isothermal adsorption models. The Langmuir model describes monolayer adsorption with uniformly distributed adsorption sites, while the Freundlich model simulates multi-layer physicochemical adsorption on heterogeneous surfaces. The Langmuir model assumes no interaction between the adsorbates, while the Freundlich model is an empirical model with limited applicability. The Langmuir-Freundlich model accounts for the interaction between adsorbates and applies to a wide range of adsorption systems [25]. The above models are defined as follows.

Langmuir model

$$Q_e = \frac{Q_m b C_e}{1 + b C_e} \quad (6)$$

Freundlich model

$$Q_e = K_f C_e^{1/n} \quad (7)$$

Langmuir-Freundlich model

$$Q_e = \frac{Q_m b C_e^n}{1 + b C_e^n} \quad (8)$$

In the above equations, Q_e and Q_m are the equilibrium adsorption amount and the maximum adsorption capacity of the adsorbent, Ce refers to the equilibrium adsorbate concentration, b is the adsorption equilibrium constant, K_f is the Freundlich constant, and n is the heterogeneity index.

Table 2 presents the fitting results of the three models. In Table 2, the Langmuir-Freundlich model provided a better fit for the adsorption of phosphorus on C-LDH and C-LDO than the other two models, suggesting that the adsorption behavior was a physicochemical process. The n value of the two adsorbents was lower than 1, indicating that phosphate adsorption was favorable and heterogeneous [26]. The theoretical maximum adsorption capacity of C-LDO was 124.1 mg/g, almost

Table 1. Kinetic parameters of different models.

Samples	Pseudo-first-order model			Pseudo-second-order model		
	Q_e (mg/g)	K_1	R^2	Q_e (mg/g)	K_2	R^2
C-LDH	66.7	1.330	0.886	71.1	0.029	0.985
C-LDO	113.7	0.940	0.906	123.1	0.011	0.990

Table 2. Fitting results of isotherm adsorption models.

Sample	Langmuir model			Freundlich model			Langmuir-Freundlich model			
	Q_m (mg/g)	B (L/mg)	R^2	$1/n$	K_f	R^2	Q_m (mg/g)	B (L/mg)	n	R^2
C-LDH	73.4	0.077	0.974	0.224	18.7	0.903	76.1	0.121	0.808	0.981
C-LDO	121.0	0.109	0.992	0.246	27.7	0.901	124.1	0.138	0.860	0.994

twice that of C-LDH. The higher adsorption capacity of C-LDO may be attributed to the increase in the specific surface area of the material and the enhanced exposure of active sites following calcination.

Site energy distribution theory proposed the site energy and the corresponding energy distribution of the adsorbent surface, which assisted in explaining the adsorption mechanism of heterogeneous surfaces [27-29]. The relationship between site energy distribution and adsorption capacity is as follows:

$$q_e(C_e) = \int_0^{\infty} q_h(E, C_e) F(E) dE \tag{9}$$

where $q_h(E, C_e)$ and $F(E)$ are the homogeneous isotherms and site energy frequency distribution over local adsorption sites with adsorption energy E, respectively. E is the site energy.

According to site energy distribution theory, adsorption energy E^* for a given adsorption site is the difference in adsorption energy between the adsorbate and solvent, which is defined by Equation (10) [30]

$$E^* = -RT \ln(C_e / C_s) \tag{10}$$

where C_s is the maximum solubility of the adsorbate. As for the phosphorus concentration at 293 K, the value is 226000 mg/L.

Based on the Langmuir-Freundlich model, the site energy distribution $F(E^*)$ was determined by differentiating the isotherm as Equation (11) [29].

$$F(E^*) = -\frac{dq_e(E^*)}{dE^*} \tag{11}$$

Equation (11) is a typical Gaussian-like distribution, where the mathematical expectation value (μ) and standard deviation (σ) are defined as Equations (12) to (14):

$$\mu(E^*) = \frac{\int_0^{+\infty} E^* \cdot F(E^*) dE^*}{\int_0^{+\infty} F(E^*) dE^*} \tag{12}$$

$$\mu(E^{*2}) = \frac{\int_0^{+\infty} E^{*2} \cdot F(E^*) dE^*}{\int_0^{+\infty} F(E^*) dE^*} \tag{13}$$

$$\sigma(E^*) = \sqrt{\mu(E^{*2}) - \mu(E^*)^2} \tag{14}$$

Fig. 3 shows the site energy and distribution of phosphorus on C-LDH or C-LDO calculated based on the Langmuir-Freundlich model. The integrated area under the curve corresponds to the maximum phosphorus adsorption capacity. As shown in Fig. 3b), the phosphorus adsorption energy distribution function $F(E^*)$ of C-LDH increased significantly after calcination, indicating that the number of C-LDO adsorption active sites formed after calcination significantly increased.

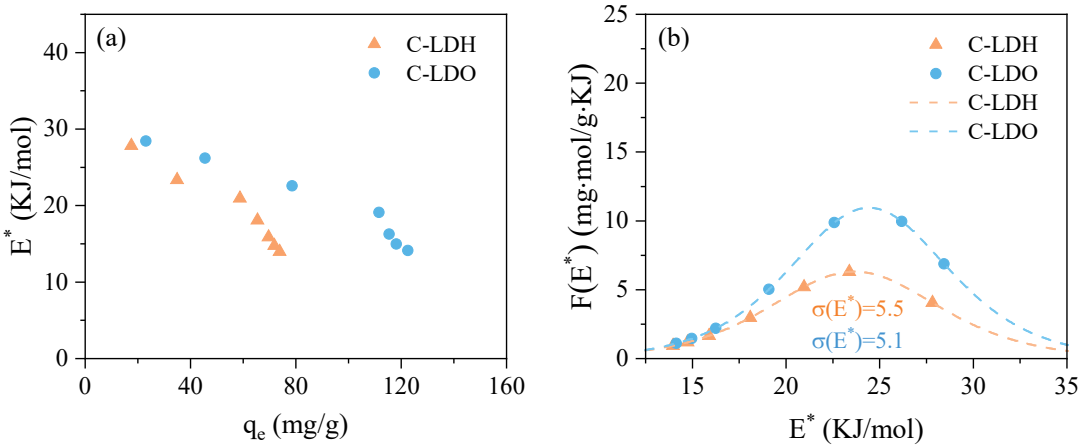

Fig. 3. Site energy and its distribution of phosphorus onto C-LDH or C-LDO. a) site energy at different P loading; b) site energy distribution.

Fig. 3a) is the relationship between E^* and q_e. It can be seen that as the adsorption amount increases, E^* decreases rapidly, suggesting that C-LDH and C-LDO first occupy high-energy adsorption sites and only transfer to low-energy sites after saturation. After calcination, the heterogeneity is slightly reduced, the width of the site energy distribution is reduced, and the site energy distribution is more concentrated. This indicates that C-LDO has a better affinity for phosphorus.

Removal Mechanism

Characterization and Analysis

Fig. 4 shows that, in addition to the typical lamellar structure of LDH, C-LDH also contains a large amount of amorphous substances (probably related to the large amount of silicon in concrete). The lamellar structure of C-LDO disappears after firing. The phosphorus removal products of C-LDH and C-LDO both contain a large amount of flaky substances, among which C-LDH-P has more flocculent substances.

XRD analysis (Fig. 4b)) shows that the crystallized product after phosphorus removal from C-LDH and C-LDO is mainly DCPD ($CaHPO_4$-$2H_2O$) (peaks 020, 12-1, 040, 14-1, 121, 150, 200, 141, 22-2, 260). The absence of hydrotalcite in the XRD pattern after phosphorus removal may be attributed to the high concentration of raw water, which leads to significant precipitation of DCPD. The resulting DCPD may overlap with or obscure the hydrotalcite peak in the XRD spectrum.

FTIR (Fig. 4c)) showed that similar absorption peaks existed at 3488 cm^{-1},1625 cm^{-1} for C-LDH and 1657 cm^{-1}, 3568 cm^{-1} for C-LDO, which were caused by the stretching vibration of the structural OH group (νOH) and the bending vibration of interlayer water molecule H-OH-H (νH_2O), in which the peaks of C-LDO at 3568 cm^{-1} were broadened and weakened, indicating that part of the interlayer water molecule and interlayer hydroxyl group were lost during the calcination process. Calcination changes the lattice vibration modes of M-OH (M: Ca, Al, and a small amount of Mg, Fe) to the stretching vibration of M-O and the bending vibration of M-O-M. These changes are reflected in the FTIR spectra, with C-LDH-P exhibiting absorption bands in the range of 427 to 1080 cm^{-1} and C-LDO-P showing a broad band spanning from 461 to 1080 cm^{-1}. The disappearance of the peak at 1420 cm^{-1} after phosphorus removal by C-LDO may be due to the reaction of CO_3^{2-} during phosphorus removal.

The infrared spectral analysis shows that the lamellar structure of C-LDH collapsed, and the M-OH vibration disappeared into M-O stretching and M-O-M bending vibration after calcination, but the M-OH lattice peaks reappeared after putting it into phosphorus solution for phosphorus removal, which represents that the lamellar structure was restored to a certain extent. The positions and intensities of the peaks indicate that the two phosphorus removers produce largely comparable yet distinguishable phosphorus-containing products after phosphorus removal, which is related to the amount of phosphorus removed and the binding affinity for phosphorus.

The phosphorus removal products of C-LDH and C-LDO were analyzed for acidic (initial pH 3) and neutral (initial pH 7) raw waters, respectively. The results are shown in Fig. 4d). Under acidic conditions, the phosphorus removal products were dominated by Fe/Al-P, while the proportion of Ca/Mg-P increased significantly as pH increased.

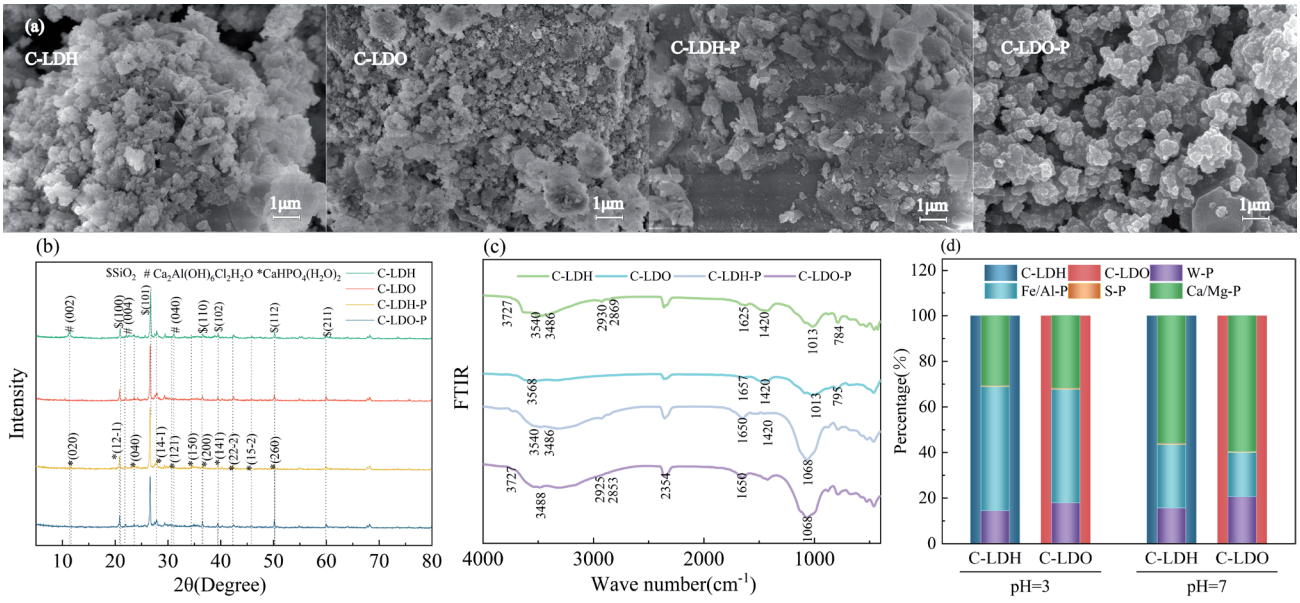

Fig. 4. a) SEM images, b) XRD, c) FTIR, and d) chemical extraction of C-LDH and C-LDO before and after phosphorus removal.

Schematic Diagram of P Removal by C-LDH

The phosphorus removal mechanism of C-LDH/C-LDO is shown in Fig. 5. The physical adsorption involves van der Waals force and electrostatic attraction between C-LDH/C-LDO and phosphate ions, as well as hydrogen bonding between adsorbent surface groups and adsorbate. In the sequential extraction test, the proportion of weakly bound phosphorus was 5-20%, and it was mostly physisorption. Interlayer anion exchange enables phosphate removal by replacing interlayer anions in Ca/Al-LDH with phosphate ions. In acidic conditions, Ca/Al-LDH dissolves, releasing Ca^{2+}, Al^{3+}, Fe^{3+}, and Mg^{2+}, which react with PO_4^{3-} to form precipitates like DCPD and $AlPO_4$. Additionally, insoluble Mg/Al-LDH and amorphous $Al(OH)_3$ adsorb phosphorus via surface adsorption or ion exchange [31]. For example, as shown in Equation (16), hydrotalcite-like compounds decompose to release free Ca^{2+} ions. In acidic raw water, these Ca^{2+} ions can react with phosphate ions, primarily through the precipitation reaction described by Equation (17), while Equations (18) and (19) may also play a minor role.

$$Ca_2Al(OH)_6Cl\cdot 2H_2O \rightarrow Ca^{2+} + Ca_aFeO_{1-b}(OH)_{2a+2b}\cdot xH_2O + OH^- + H_2O \quad (16)$$

$$Ca^{2+} + HPO_4^{2-} + 2H_2O \rightarrow CaHPO_4\cdot 2H_2O \quad (17)$$

$$3Ca^{2+} + 2PO_4^{3-} \rightarrow Ca_3(PO_4)_2 \quad (18)$$

$$8Ca^{2+} + 4PO_4^{3-} + 2HPO_4^{2-} \rightarrow Ca_8H_2(PO_4)_6 \quad (19)$$

Conclusions

C-LDH and C-LDO exhibited effective phosphorus removal performance in acidic phosphorus-containing raw water, with optimal pH values of 4 and 3, respectively. Under these conditions, the presence of coexisting anions had varying effects on phosphorus removal: NO_3^-, Cl^-, and SO_4^{2-} showed negligible interference, whereas the impact of CO_3^{2-} became more significant with increasing concentration. The phosphorus adsorption equilibrium was achieved within 12 to 16 hours, and the adsorption process followed a quasi-two-stage kinetic model. The phosphorus adsorption process by C-LDH/C-LDO conformed to the Langmuir isotherm model, with a maximum adsorption capacity of 164.01 mg/g. The phosphorus removal mechanism of C-LDH/C-LDO primarily involved the precipitation and complexation of Ca^{2+}, Mg^{2+}, and Al^{3+} with phosphate ions, as well as electrostatic attraction and interlayer anion exchange. The phosphorus removal products mainly consisted of S-P, Ca/Mg-P, and Al-P, accounting for 99% of the total adsorbed phosphorus. At low pH, the proportion of Al-P in the products was relatively high; however, as the pH increased, the proportion of Ca/Mg-P increased significantly and became dominant.

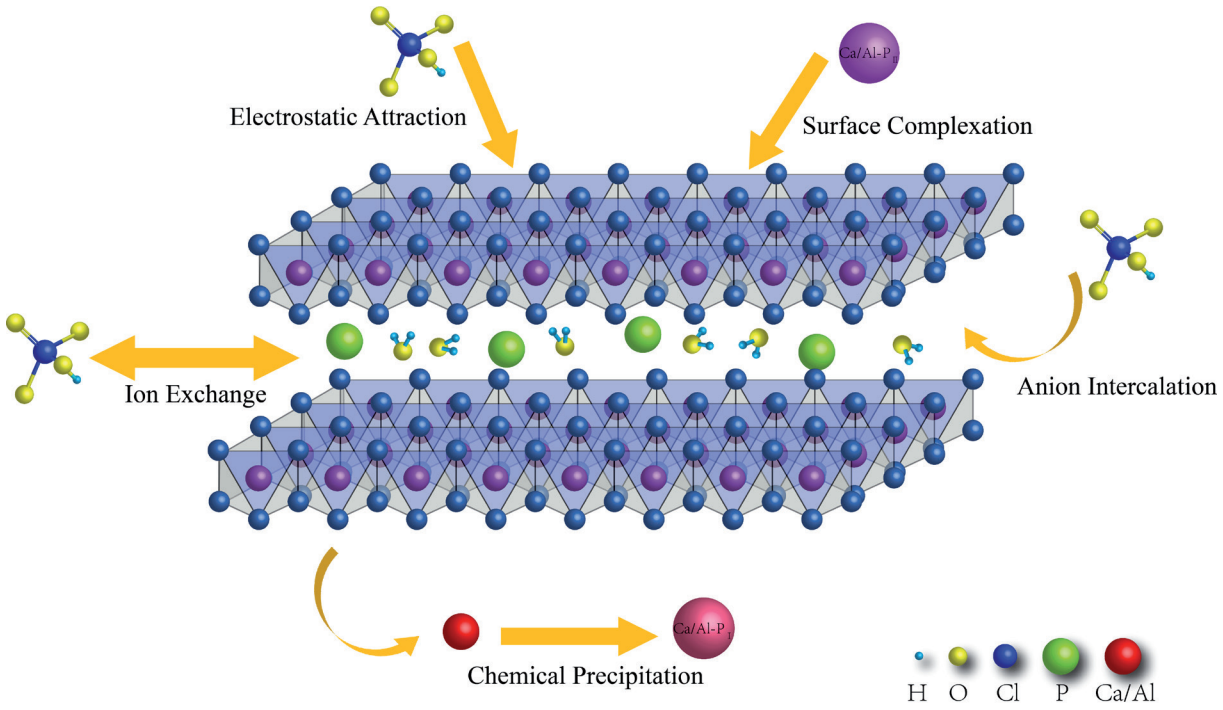

Fig. 5. Mechanism of phosphorus removal by CLDH/CLDO.

Conflict of Interest

The authors declare no conflict of interest.

References

1. ZENG G.Y., LI G.Y., WU Y., TANG C.F., YUAN W.Y., ZHONG H.X., DENG N., LIU Q.Z., LIU J.W., OUYANG K., HU X.J., YANG X. Preparation of high specific surface area Zn/Al/Zr LDH@HTCC for enrichment and recovery of phosphorus from water. Surf Interfaces. **42** (PA), 103330, **2023**.
2. ATANGANA NJOCK P.G., ZHOU A.N., YIN Z.Y., SHEN S.L. Integrated risk assessment approach for eutrophication in coastal waters: case of Baltic Sea. Journal of Cleaner Production. **387**, 135673, **2023**.
3. LEE Y.S., CHOI J., SONG G.K., CHOI K., LEE J.Y., JUNG K-W. Adsorption and mechanistic study for phosphate removal by rice husk-derived biochar functionalized with Mg/Al-calcined layered double hydroxides via co-pyrolysis. Composites Part B. **176**, 107209, **2019**.
4. HUANG H.M., LIU J.H., ZHANG P., ZHANG D.D., GAO F.M. Investigation on the simultaneous removal of fluoride, ammonia nitrogen, and phosphate from semiconductor wastewater using chemical precipitation. Chemical Engineering Journal. **307**, 696, **2017**.
5. LUO D., WANG L.Y., NAN H.Y., CAO Y.J., WANG H., KUMAR T.V., WANG C.Q. Phosphorus adsorption by functionalized biochar: a review. Environmental Chemistry Letters. **21**, 497, **2023**.
6. ZHANG J.M., HUANG W.Q., YANG D.X., XIANG J.L., CHEN Y. Removal and recovery of phosphorus from secondary effluent using layered double hydroxide-biochar composites. Science of the Total Environment. **844**, 156802, **2022**.
7. SÜRMELI M., YAZICI H., KILIÇ M., KARABOYACI M. Screening of optimum composition of superparamagnetic nanocomposite microparticles modified with various layered double hydroxides for phosphorus removal. Journal of Water Process Engineering. **49**, 103001, **2022**.
8. WANG T.T., YANG Z.H., YANG B., WANG R.J., HUANG J.H. The electrochemical performances of Zn–Sn–Al-hydrotalcites in Zn–Ni secondary cells. Journal of Power Sources. **257**, 174, **2014**.
9. PORNTHIP W., RACHNARIN N., JORDI L. Application of Fe–Zn–Mg–Al–O hydrotalcites supported Au as active nano-catalyst for fermentative hydrogen production. Chemical Engineering Journal. **253**, 148, **2014**.
10. ZHANG X.L., GUO L., HUANG H.L., JIANG Y.H., LI M., LENG Y.J. Removal of phosphorus by the core-shell bio-ceramic/Zn-layered double hydroxides (LDHs) composites for municipal wastewater treatment in constructed rapid infiltration system. Water Research. **96**, 280, **2016**.
11. WILLIAMS J.D.H., SHEAR H., THOMAS R.L. Availability to scenedesmus quadricauda of different forms of phosphorus in sedimentary materials from the great Lakes1. Limnology and Oceanography. **25**, 1, **1980**.
12. SOMMERS L.E., HARRIS R.F., WILLIAMS J.D.H., ARMSTRONG D.E., SYERS J.K. Fractionation of organic phosphorus in lake sediments. Soil Science Society of America Journal. **36**, 51, **1972**.
13. EHAMA M., HASHIHAMA F., KINOUCHI S., KANDA J., SAITO H. Sensitive determination of total particulate phosphorus and particulate inorganic phosphorus in seawater using liquid waveguide spectrophotometry. Talanta. **153**, 66, **2016**.
14. KANG L., MUCCI M., LVRLING M. Influence of temperature and pH on phosphate removal efficiency of different sorbents used in lake restoration. Science of the Total Environment. **812**, 151489, **2022**.
15. GUO Q.X., YIN C.B., CHEN Y.Z., FANG Z.Y., XIAO H., HE J.S., HUANG L.P., WU G.X., ZENG Z.X., SHEN F., DENG S.H., JI F.Y., FANG D.X. Periodic pH regulation controls the phosphate uptake-release behavior and structural evolution of layered double hydroxides. Chemical Engineering Journal. **459**, 141584, **2023**.
16. LIU C., ZHANG M.Y., PAN G., LUNDEHØJ L., NIELSEN U.G., SHI Y., HANSEN H.C.B. Phosphate capture by ultrathin MgAl layered double hydroxide nanoparticles. Applied Clay Science. **177**, 82, **2019**.
17. YANG F., ZHANG S., SUN Y., TSANG D.C.W., CHENG K., OK Y.S. Assembling biochar with various layered double hydroxides for enhancement of phosphorus recovery. Journal of Hazardous Materials. **365**, 665, **2019**.
18. VU C.T., WU T.T. Magnetic porous NiLa-layered double oxides (LDOs) with improved phosphate adsorption and antibacterial activity for treatment of secondary effluent. Water Research. **175**, 115679, **2020**.
19. JOBBÁGY M., REGAZZONI A.E. Dissolution of nano-size Mg–Al–Cl hydrotalcite in aqueous media. Applied Clay Science. **51** (3), 366, **2011**.
20. LI R.H., WANG J.J., ZHOU B.Y., AWASTHI M.K., ALI A., ZHANG Z.Q., GASTON L.A., LAHORI A.H., MAHAR A. Enhancing phosphate adsorption by Mg/Al layered double hydroxide functionalized biochar with different Mg/Al ratios. Science of the Total Environment. **559**, 121, **2016**.
21. LV L., HE J., WEI M., DUAN X. Kinetic studies on fluoride removal by calcined layered double hydroxides. Industrial & Engineering Chemistry Research. **45**, 8623, **2006**.
22. XIAO L.O., LI Y., KONG Q.P., LAN Y.L. From wastes to functions: preparation of layered double hydroxides from industrial waste and its removal performance towards phosphates. Environmental Science and Pollution Research. **29**, 11893, **2022**.
23. YANG G.D., TANG L., LEI X.X., ZENG G.M., CAI Y., WEI X., ZHOU Y.Y., LI S.S., FANG Y., ZHANG Y. Cd(II) removal from aqueous solution by adsorption on α-ketoglutaric acid-modified magnetic chitosan. Applied Surface Science. **292**, 710, **2014**.
24. QIU S.K., ZHAO D., FENG Y.Y., LI M.M., LIANG X.F., ZHANG L.S., LUO Y., ZHANG K.Q., WANG F. Adsorption performance and mechanism of Ca–Al-LDHs prepared by oyster shell and pop can for phosphate from aqueous solutions. Journal of Environmental Management. **303**, 114235, **2022**.
25. AL-GHOUTI M.A., DA'ANA D.A. Guidelines for the use and interpretation of adsorption isotherm models: a review. Journal of Hazardous Materials. **393**, 122383, **2020**.
26. SANTOS A.F., ARIM A.L., LOPES D.V., GANDO-FERREIRA L.M., QUINA M.J. Recovery of phosphate from aqueous solutions using calcined eggshell as an eco-friendly adsorbent. Journal of Environmental Management. **238**, 451, **2019**.
27. REGUYAL F., SARMAH A.K. Site energy distribution analysis and influence of Fe_3O_4 nanoparticles on sulfamethoxazole sorption in aqueous solution by magnetic pine sawdust biochar. Environmental Pollution. **233**, 510, **2018**.

28. YAN B., NIU C.H., WANG J. Kinetics, electron-donor-acceptor interactions, and site energy distribution analyses of norfloxacin adsorption on pretreated barley straw. Chemical Engineering Journal. **330**, 1211, **2017**.
29. HE J., GUO J.S., ZHOU Q.H., YANG J.X., FANG F., HUANG Y. Analysis of 17α-ethinylestradiol and bisphenol a adsorption on anthracite surfaces by site energy distribution. Chemosphere. **216**, 59, **2019**.
30. YAN B., NIU C.H. Modeling and site energy distribution analysis of levofloxacin sorption by biosorbents. Chemical Engineering Journal. **307**, 631, **2017**.
31. LUNDEHØJ L., CELLIER J., FORANO C., NIELSEN U.G. Atomic level understanding of orthophosphate adsorption by magnesium aluminum-layered double hydroxides – a multitechnique study. The Journal of Physical Chemistry C. **123** (39), 24039, **2019**.